The role of carbon species in heterogeneous catalytic processes: an *in situ* soft x-ray photoelectron spectroscopy study

2008 J. Phys.: Condens. Matter 20 184016

(http://iopscience.iop.org/0953-8984/20/18/184016)

IOP Publishing Journal of Physics: Condensed Matter

J. Phys.: Condens. Matter **20** (2008) 184016 (13pp) doi:10.1088/0953-8984/20/18/184016

The role of carbon species in heterogeneous catalytic processes: an *in situ* soft x-ray photoelectron spectroscopy study

E M Vass, M Hävecker, S Zafeiratos, D Teschner, A Knop-Gericke[1] and R Schlögl

Fritz-Haber-Institut der Max-Planck-Gesellschaft, Department of Inorganic Chemistry, Faradayweg 4-6, D-14195 Berlin, Germany

E-mail: knop@fhi-berlin.mpg.de

Received 15 October 2007, in final form 2 January 2008
Published 17 April 2008
Online at stacks.iop.org/JPhysCM/20/184016

Abstract

High pressure x-ray photoelectron spectroscopy (XPS) is used to characterize heterogeneous catalytic processes. The success of the new technique is based on the possibility of correlating the catalytic activity and the electronic structure of an active surface. The dynamic character of a catalyst surface can be demonstrated impressively by this technique. In this contribution the basics of high pressure XPS will be discussed. Three examples of heterogeneous catalytic reactions are presented in this contribution: the selective hydrogenation of 1-pentyne and the oxidation of ethylene over Pd based catalysts and the dehydrogenation of *n*-butane over V based catalysts.

It is shown that the formation of subsurface carbons plays an important role in all the examples. The carbon incorporated changes the electronic structure of the surface and so controls the selectivity of the reaction. A change of the educts in the reaction atmosphere induces modifications of the electronic surface structure of the operation catalysts.

(Some figures in this article are in colour only in the electronic version)

1. Introduction

Obviously, the understanding of the interaction of a catalyst's surface with the reactants plays a key role in a detailed description of catalytic processes. However, a spectroscopic characterization of the reacting surface under ambient conditions is challenging. While photon-in photon-out techniques can be applied at high gas pressures, they typically show a lack of surface sensitivity. Photon-in electron-out techniques like XPS on the other hand are intrinsically more surface sensitive due to the strong interaction of (low energy) electrons with matter but they suffer, for the same reason, from limitations in the pressure of the ambient gas due to the strong scattering of the outgoing electron in the gas phase. Thus, XPS has been typically applied only under UHV or HV conditions, i.e. far away from normal operation conditions of a catalyst.

Nevertheless, recent methodological developments [1–7] make it feasible to expand the operation range of XPS by several magnitudes in pressure from UHV conditions to ambient pressure in the mbar range. The use of XPS as a tool for characterization of catalysts is attractive for several obvious reasons. XPS shows a universal chemical sensitivity by probing the different core levels of the elements. It can detect all elements except for hydrogen in all their different electronic states, e.g. XPS is not limited to certain specific valences of an element. The surface sensitivity of XPS critically depends on the kinetic energy of the released photoelectrons and thus on the energy difference between the incoming photon and the binding energy of the core level. Low energy electrons of 50–150 eV show the smallest inelastic mean free path

[1] Author to whom any correspondence should be addressed.

(IMPF) in a solid and thus the highest surface sensitivity [8]. Thus, XPS develops into an ultimate surface sensitive tool for characterizing the topmost layers of a material when it is operated with a tunable x-ray source at a storage ring. Synchrotron based XPS makes it feasible to ensure a low kinetic energy of the released photoelectrons for all core levels. To exemplify this fact it is useful consider that the IMFP e.g. in V_2O_5 for V 2p photoelectrons is 17.7 Å when excited with Mg Kα radiation (i.e. a standard x-ray tube, $h\nu = 1253.4$ eV) and just 6.6 Å when the kinetic energy of the electrons is 150 eV (i.e. $h\nu = 670$ eV). Excitation of the C 1s core level in a carbon matrix results in an IMFP of 28 Å and 8.6 Å for $h\nu = 1253.4$ eV and 330 eV, respectively (values calculated according to the Penn *et al* algorithm TPP-2m [8]). In addition, the element sensitivity is increased due to the enhancement of the ionization cross section at excitation energies close to the threshold: V 2p: 0.2 Mb for $h\nu = 1253$ eV versus 1 Mb for $h\nu = 670$ eV; C 1s: 0.02 Mb for $h\nu = 1253$ eV versus 0.6 Mb for $h\nu = 330$ eV [9].

Synchrotron based XPS allows also for specific modes of depth resolution when the same core level is investigated with varying photon energies resulting in different kinetic energies of the photoelectron, i.e. different information depths for the same element. Thus, there is a smart way of 'element depth profiling' without destruction of the surface. While direct interaction of the reactants with the catalyst takes place only on the outermost surface layer species in near surface layers ('subsurface') often play an important role in modifying the electronic structure on the outermost surface and thus creating modified sites for adsorption or reaction. Furthermore, subsurface species might play a role as a reservoir for surface species, as well. Examples will be given in this report.

In addition, synchrotron based XPS shows a superior energy resolution compared to XPS based on standard (i.e. non-monochromatic) laboratory x-ray tubes due to the small bandwidth of the excitation source.

The use of synchrotron radiation facilities allows the differentiation between effects of two and three dimensional layer growth on the shift and broadening of XPS lines, due to high energy resolution and tunable photon energy. It is well known that there is an effect of the layer thickness on the full width at half maximum (FWHM) and on the energy position of XPS lines. Himpsel *et al* have shown that the oxidation state of Si in a 14 Å thick silicon oxide layer grown on Si(111) changes as a function of the photon energy [10]. In this study different photon energies were used to measure the Si $2p_{3/2}$ core level of the oxide layer. With photon energy of 130 eV it was observed that the Si^{3+} contribution is enhanced relative to Si^{1+} and Si^{2+} contributions [10]. The authors declare this effect partly from the location of the Si^{3+} species closer to the surface and therefore the corresponding XPS signal is more pronounced at 130 eV compared to more bulk sensitive measurement with 400 eV [10]. Thus the FWHM of an XPS line which might be the envelope curve of several different oxidation states changes as a function of layer thickness and therefore changes with the morphology. Since the binding energies of different oxidation states might be different as well, shifts in the energy positions of XPS lines might be observed. These arguments are not only valid for oxides. In general shifts and changes in the broadening of XPS lines will be expected in all system showing inhomogeneities of the chemical bonding in the layer and particle as a function of thickness and size, respectively.

There exist however artificial effects on the shift and broadening of XPS lines. Charging of the sample investigated influences at least the energy position of the XPS line. In the case of inhomogeneous charging the FWHM of the XPS lines might be enhanced as well. Charging might be reduced in gas phase atmospheres, because the ionization of gas phase molecules due to absorption processes creates charge, which compensates partly the charging of the sample.

Another point that will be highlighted in this report is the importance of chemical complexity. Certainly, 'simple' model systems are necessary to gain deeper insight into elementary steps of catalytic reactions (e.g. oxygen activation). Working at reduced temperatures and pressures is extremely useful for eventually slowing down processes. But to evaluate without assumptions whether the species found are indeed involved in the reaction is only possible with the real material under relevant conditions. The examples presented in this article clearly show that *in situ* XPS can be applied not only to model systems but also to real supported catalysts. Since the support of a real catalyst is usually an isolating material like alumina, silica, titania, etc, special care has to be taken for the calibration of the binding energy scale in the case of charging.

Most of the reactions that are studied by *in situ* XPS take place at different (i.e. higher) pressure when tested in a reactor (normal operation conditions). Thus, it needs to be proven that the catalyst surface at the conditions applied for the spectroscopic characterization acts in the same way as under normal operation conditions. Macroscopically, this is reflected in the selectivity of the reaction. This implies: (A) the products need to be determined during the spectroscopic investigation; (B) it is highly advantageous if the chemical reaction under investigation allows for different reaction pathways so that the branching ratio (i.e. the selectivity) might be evaluated. This branching ratio might serve as a macroscopic fingerprint of the surface state. If a reaction under normal operation conditions can be mimicked in the above mentioned way, the actual reaction parameters (e.g. pressure, mixing ratio of reactants, temperature) might be chosen differently to the normal operation conditions without corrupting the relevance of the results obtained. Thereby, meaningful relationships between the electronic structure and the functionality of the material can be obtained ('structure–activity relationship').

To clarify and to demonstrate the points mentioned in the introduction, three examples will be discussed in the following. All of them elucidate the role of carbon on the surface of the catalysts and therefore on the catalytic event.

A study of Pd based catalysts used in selective hydrogenation of 1-pentyne will highlight the role of carbon deposits and carbon subsurface layers in the selectivity of the reaction. The second section, closely related to the previous section, studies the oxidation of ethylene on Pd(111) single crystal. Similarities between the two reactions will be pointed out.

Finally, in the third example V based catalyst in the dehydrogenation of *n*-butane will be described in detail. In that

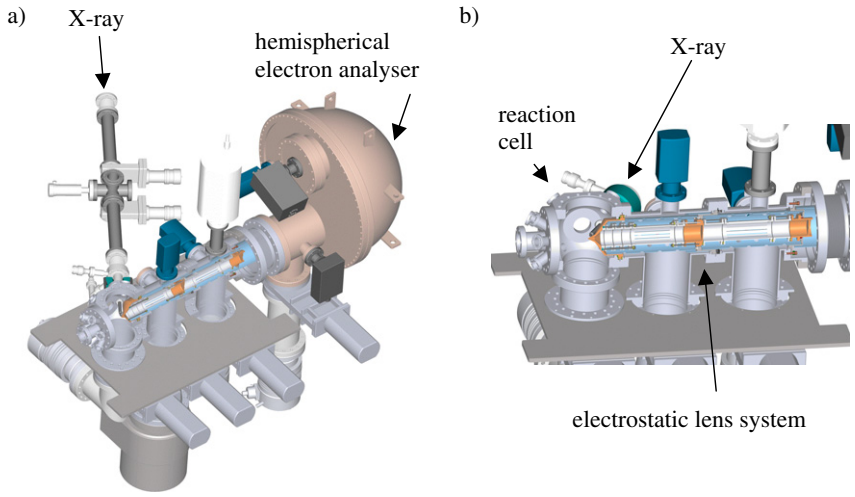

Figure 1. Schematic layout of the high pressure XPS system. In (b) a detailed sketch of the reaction cell and the electrostatic lens system is shown.

case C deposits block the surface and deactivate the catalyst. Strategies for avoiding the activity loss due to coking and their impact on the catalysts electronic structure are discussed.

2. Experimental details

The experiments have been performed at the synchrotron radiation facility BESSY (Berliner Elektronenspeicherringgesellschaft für Synchrotronstrahlung) located in Berlin using the high brilliance radiation of the undulator U49/2 as an x-ray source [11–13]. *In situ* XP spectra were obtained using the high pressure XPS station designed and constructed at the FHI. Details of the set-up are described elsewhere [7]. A sketch of the set-up and a close-up of the experimental cell and the differentially pumped electrostatic lens system are shown in figures 1(a) and (b).

In brief, the samples (e.g. single crystals, polycrystalline foils, pressed powders) are mounted inside a reaction cell onto a sapphire sample holder approximately 2 mm in front of the first aperture of a differentially pumped electrostatic lens system. The homebuilt electron lens serves as the input system for a (modified) commercial hemispherical electron analyzer (PHOIBOS 150, Specs-GmbH). X-rays enter at 55° relative to the electron analyzer axis. A variety of gases can be introduced to the cell and the gas phase composition is monitored via mass spectrometer simultaneously with the spectroscopic characterization by XPS. Heating is provided by a NIR laser at the rear of the sample and monitored by a thermocouple attached directly to the sample surface.

3. Case studies

3.1. 1-pentyne hydrogenation on Pd based catalysts

In this part the influence of C deposit on one catalytic performance of selective 1-pentyne hydrogenation will be discussed. The formation of a surface/subsurface Pd–C phase is observed. A similar phase is observed in the case of the ethylene oxidation over Pd as described in section 3.2. In both cases, the subsurface C layer influences the selectivity of the reaction.

The influence on the catalytic properties of carbon residing in the subsurface region was described previously [14–16]. Since these are all *ex situ* studies the question of stability of intermediates is an issue. Most of these species are metastable and form only under reaction conditions. It was shown experimentally that the adsorbed C atoms have to overcome an activation barrier of 107 kJ mol^{-1} to penetrate the Pd bulk [17]. DFT calculations revealed an activation energy of 59–78 kJ mol^{-1} [18]. The C atoms then become energetically stabilized in the subsurface bulk dissolved state, whereas the C migration inside the Pd bulk has a considerably lower activation barrier at 65 kJ mol^{-1} [19]. The amount of carbon within the first few layers will depend strongly on temperature, pressure and time on stream. A UHV study allowed quantification of the carbon uptake from ethane dissociation through the surface Pd layer [17]. But in this investigation it was not possible to measure the distribution of carbon among near-surface and deeper bulk regions. *In situ* x-ray photoelectron spectroscopy using tunable synchrotron light can be used to monitor the concentration profile of species involved perpendicular to the surface as described in section 1.

Four different catalysts have been investigated by *in situ* XPS under selective hydrogenation reaction conditions (0.85 mbar H_2 + 0.05 mbar 1-pentyne at 358 K) of 1-pentyne [20]. All samples showed catalytic activity in the hydrogenation of 1-pentyne in the mbar pressure range as indicated in table 1. Pd(111) produces only pentene, whereas the other catalysts form products related to single and total hydrogenation.

Figure 2 shows the Pd $3d_{5/2}$ core level spectra of (a) Pd(111), (b) Pd foil, and (c) 5% Pd/CNT in the reaction mixture. For comparison the Pd $3d_{5/2}$ core level of a Pd foil in 0.2 mbar trans-2-pentene + 0.6 mbar H_2 is shown. Carbonaceous adsorbed species induced a shift of the surface core level to higher binding energy (BE) of 335.7 eV compared

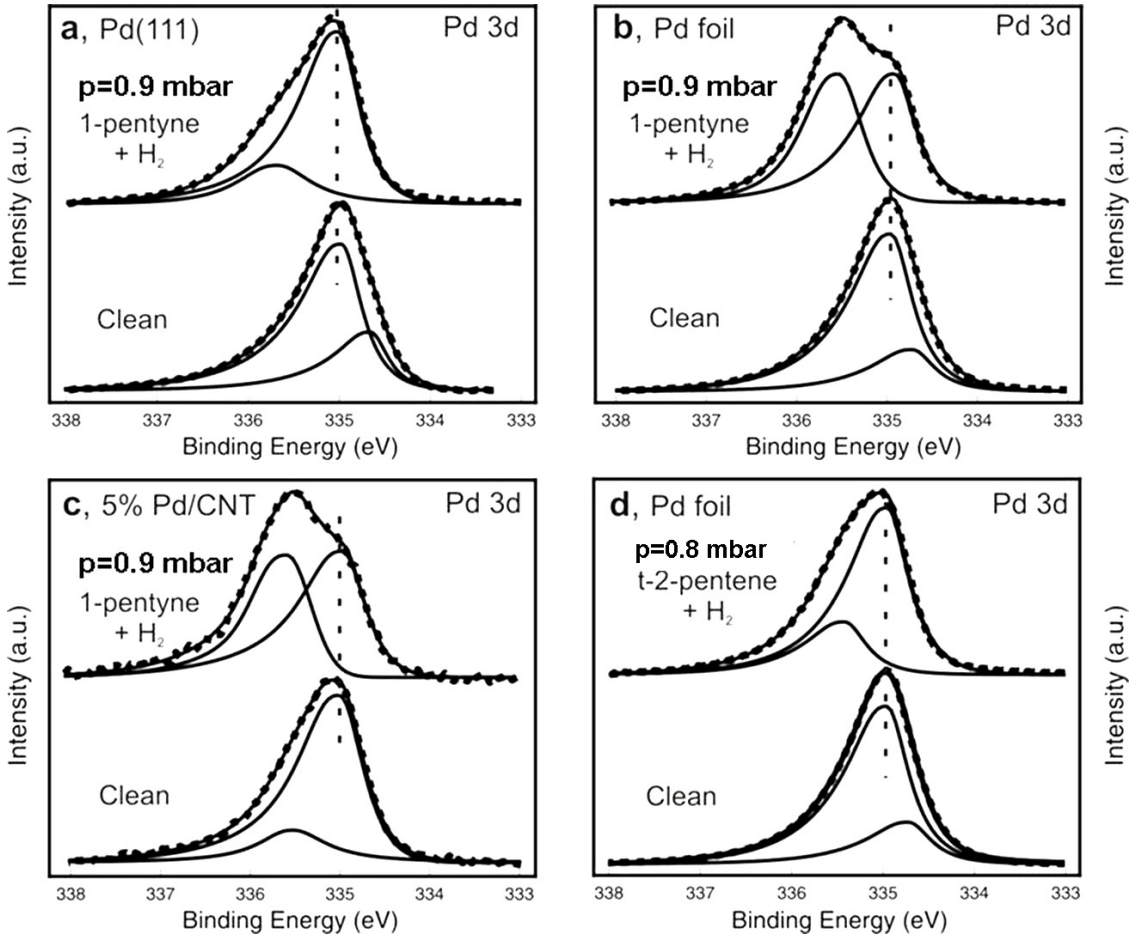

Figure 2. Pd $3d_{5/2}$ of (a) Pd(111), (b) Pd foil, (c) 5% Pd/CNT in the reaction mixture of 0.85 mbar H_2 + 0.05 mbar 1-pentyne at 358 K. The incident photon energy was 720 eV. Dashed line: measured data, full line: fits. As a comparison, Pd 3d of Pd foil during the hydrogenation of trans-2-pentene (0.2 mbar trans-2-pentene + 0.6 mbar H_2) is shown in (d) [20].

Table 1. Conversion and selectivities in 1-pentyne hydrogenation over various catalysts at 0.9 mbar conditions at 358 K.

	5% Pd/CNT	3% Pd/Al_2O_3	Pd foil	Pd(111)
Conversion (%)	10	5	2.5	<1
Selectivity pentene (%)	95	80	98	100
Selectivity pentane (%)	5	20	2	—

to the bulk palladium signal (∼335.0 eV) [21]. The structure at 334.7 eV in the spectra of the clean Pd(111) and foil surfaces is due to the surface core level shift [20]. The Pd foil and the supported catalyst show at 335.6 eV a palladium peak with significantly higher intensity compared to Pd(111). In the hydrogenation of trans-2-pentene on Pd foil this intense new component at 335.6 eV did not form; only adsorbate induced states at 335.7 eV formed. The valence band spectra (not shown) of the Pd foil taken during hydrogenation of 1-pentyne indicates a redistribution of the spectral weight in the valence band. The intensity of higher lying levels of the Pd d band decreased while a new band at 6 eV developed [20].

Figure 3 shows XP spectra of a Pd foil under reaction conditions using different photon energies and thus different information depths. From this figure the authors concluded that the component at 335.6 eV is located in the outermost Pd surface layers. The possibility of the formation of a β-hydride can be excluded since its BE is given by 335.2 eV in [22]. A simple calculation allows the authors to conclude that the new component has a thickness of 2–3 Pd atomic layers. Further calculations on C depth profile showed, that there is not only a carbon layer on top of the Pd foil. Therefore this component was assigned to a Pd state modified by dissolved C in the top few layers.

The change of the electronic structure of the catalysts is related to changes in the geometric structure. High resolution TEM pictures have indicated the Pd lattice fringes near the surface being expanded by a few per cent in comparison with Pd bulk values [23].

The carbon phase was investigated in detail by *in situ* XPS. These measurements demonstrate the metastable character of the Pd–C phase, since this phase partly decomposed in the absence of 1-pentyne gas phase above the sample surface.

The C 1s spectrum during reaction (curve 1 in figure 4(a)) shows a maximum at 284.6 eV with a shoulder at 283.4 eV. The latter BE is close to that of carbides [21]. As the 1-pentyne is switched off the low BE shoulder disappears and

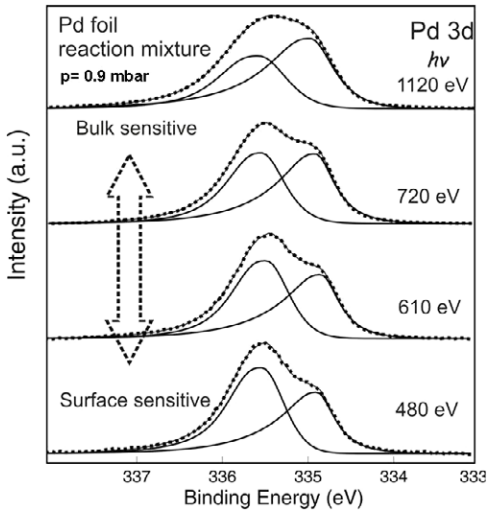

Figure 3. Non-destructive depth profile experiment on the Pd $3d_{5/2}$ core level of Pd foil during 1-pentyne hydrogenation (0.85 mbar H_2 + 0.05 mbar 1-pentyne at 358 K) [20].

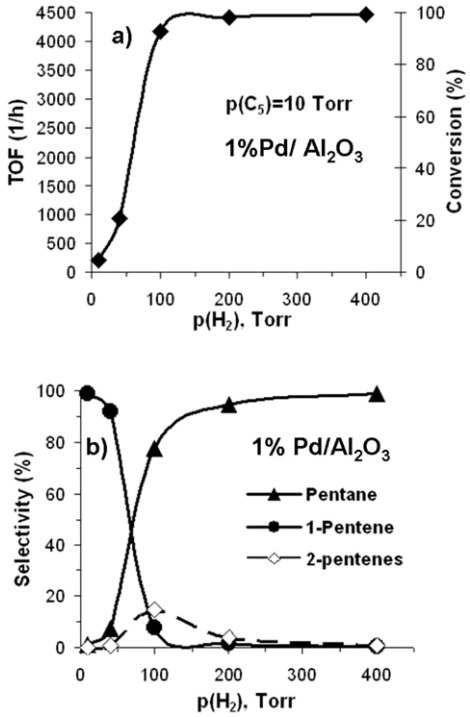

Figure 5. 1-pentyne hydrogenation over 1% Pd/Al_2O_3 in a closed loop reactor. The partial pressure of 1-pentyne was 10 Torr. (a) Conversion, (b) selectivity [20].

the intensity of the main peak decreases resulting in a shift of the peak to 284.4 eV (curve 2). It is remarkable that the time constants of the two reduction processes are different. The main peak loses intensity instantaneously, whereas the shoulder at lower binding energies disappeared after several minutes. This is a clear indication that the two peaks are due to two discrete species, which are not directly related. The difference spectrum (curves 1, 2) in figure 4(a) shows an asymmetry of the peak at 284.8 eV. Since the gas phase does not contribute within this energy range as shown by curve 4 in figure 4(a) the peak is attributed to chemisorbed pentyne molecules on Pd, which desorb as the pentyne feed is switched off. The switch off experiments have shown that pentyne is adsorbed on the Pd–C phase.

The Pd 3d spectra corresponding to the above discussed C 1s spectra are shown in figure 4(b). As the pentyne is switched off, the peak assigned to the Pd–C component is partially decreased. Since the difference indicates a binding energy of 335.7 eV the Pd–C phase may be the sum of several components.

The reaction profile obtained in a closed loop reaction at constant 1-pentyne pressure of 10 Torr is shown in figure 5. Two different selectivity regimes can be identified. At low hydrogen partial pressures and low H_2:C_5 ratios the hydrogenation is selective, since 1-pentene was formed as the major product. At H_2:C_5 ratios greater than 7 the activity was significantly enhanced. Nearly full conversion was observed and the selectivity changed to total hydrogenation.

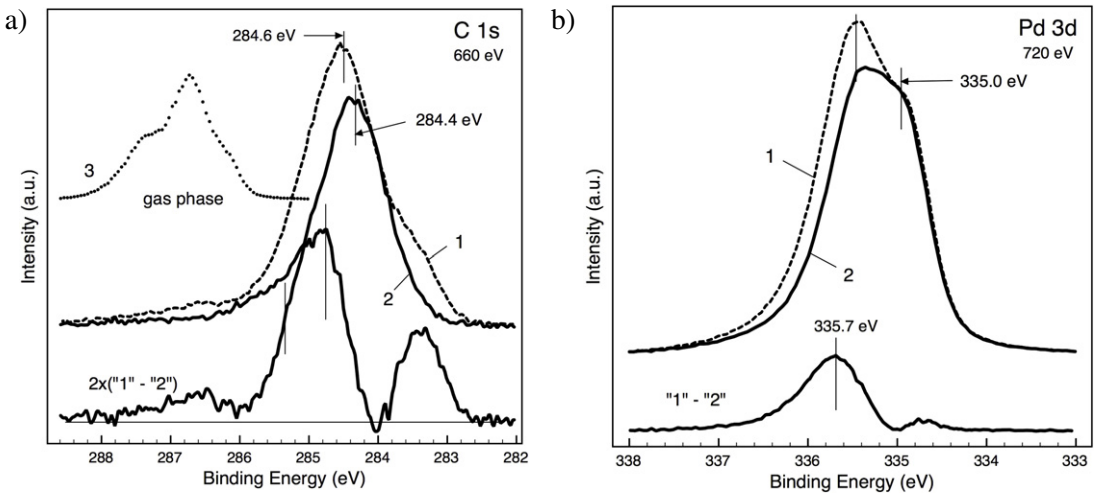

Figure 4. (a) C 1s and (b) Pd 3d regions of Pd foil at different conditions. 1: in the reaction mixture; 2: after switching off 1-pentyne (only H_2); 3: after switching off H_2 (only 1-pentyne). All spectra were recorded at 358 K. Some difference spectra are also shown [20].

Many results on the chemistry of subsurface and bulk dissolved hydrogen have been published within the last few years [24–27]. Thermal desorption spectroscopy measurements have shown that hydrogen emerging from the bulk of metal particles to the surface appears at lower temperature and is therefore more energetic and thus far more reactive than surface hydrogen [28]. But this hydrogen is too active to be selective. It was shown that bulk dissolved hydrogen is active in alkene hydrogenation or in the total hydrogenation of alkynes [27, 29]. The equilibrium between surface hydrogen and dissolved hydrogen in the volume seems to be disturbed by the formation of the Pd–C surface phase, which inhibits the repopulation of the bulk dissolved hydrogen, as well as its emergence to the surface.

The total mass change of a sample bed was measured using a tapered element oscillating microbalance (TEOM). Each hour on stream the retained mass levels were estimated after purging with helium. The gas feed was 1 bar of hydrogen and 0.1 bar of 1-pentyne. To change from total hydrogenation conditions to conditions favoring the selective hydrogenation the hydrogen was diluted from 100% to 5% with helium. It turned out that the mass uptake is a factor of five higher under selective hydrogenation conditions.

Pulses of 1-pentyne in helium were passed over 1% Pd/Al_2O_3 catalyst. The catalyst was pretreated in 1 bar hydrogen at RT to saturate the amount of hydrogen diluted in the Pd particles. The product pulses were analyzed by mass spectrometry. The first product pulse contained mainly pentene and traces of pentane. Subsequent pulses did not show any conversion. The ratio of hydrogen atoms which are required to transform the 1-pentyne to pentene and Pd atoms in the catalyst can be estimated to be 13:1 (H:Pd). This value cannot be explained by dissolved H in Pd. Therefore the substrate must play a significant role. The support was found to be inactive in the absence of palladium; hydrogen can spill over from the metal to the support. Hence there is a hydrogen reservoir, and the spilled over hydrogen can supply activated hydrogen for the reaction. In contrast to the bulk dissolved hydrogen observed in TDS measurements, surface hydrogen is selective.

The authors suggested a model of the Pd surface active in the selective hydrogenation on 1-pentyne as shown in figure 6. *In situ* XPS depth profiling showed that a carbon diluted palladium surface phase was formed in the early stage of the hydrogenation, and was composed of a thin layer of ∼3 Pd atomic layers thickness. As pentyne is switched off, the adsorbed molecules desorb and the Pd–C layer breaks up.

Selective hydrogenation of 1-pentyne was a major reaction on this modified Pd surface, since total hydrogenation was strongly inhibited by the elimination of subsurface H participating in the reaction. Further the modified surface electronic structure of Pd obviously and isolation of active sites possibly contributed to governing hydrogenation of alkynes to alkenes. Since the switch off experiments indicated the metastable character of this surface, *in situ* experiments are obligatory when aiming to reveal mechanistic details of heterogeneous hydrogenation chemistry.

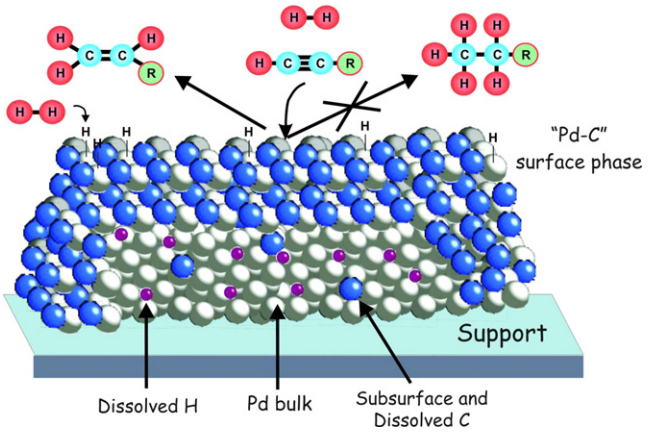

Figure 6. Model of a palladium surface during 1-pentyne hydrogenation.

A similar Pd–C surface species, which has a strong influence on the selectivity, was found during the oxidation of ethene on Pd(111). The peculiarities of this system will be described in the next example section.

3.2. Ethene oxidation on Pd based catalysts

Pd(111) has been studied during the oxidation of ethene in the pressure range of 10^{-3} mbar (5×10^{-4} mbar C_2H_4 and 1.5×10^{-3} O_2) at temperatures of 330–923 K. Figure 7(a) shows the partial pressure of carbon oxide products plotted versus temperature. The CO and CO_2 signals show strong hysteresis temperature behavior, which is a consequence of the delayed formation of the Pd–C phase during cooling [30]. The water signal is not included since the partial pressure of water follows the inverse ethene pressure multiplied by 2.

The reaction starts at $T > 430$ K, which is in agreement with previous thermal ethene decomposition studies [17]. A fine structure of the initial activity is observed. A minimum of the ethene partial pressure forms at 480 K and the selectivity for CO_2 is almost 100% since CO formation has not yet started. Between 480 and 500 K the ethene conversion is constant and the carbon dioxide formation rate decreases, reaching a local minimum at 520 K, whereas the CO formation increases at the same temperatures. The catalyst became highly active with respect to CO production. The low temperature regime (480–660 K) is characterized by a significant activity increase and a strong decrease of CO_2 selectivity and a strong increase in CO selectivity. At high temperatures (660–923 K), the activity is more or less constant and the selectivity changes are less pronounced. CO remains the main product.

Figure 7(b) shows the C 1s photoelectron spectra during the heating of the sample. In the temperature range from 330–461 K the Pd(111) surface is covered by carbon containing surface species, indicated by a broad peak between 283 and 286 eV. Binding energies between 285.53 and 285.80 eV are given in the literature for low and high CO coverage respectively [31]. Therefore, the shoulder at 285.65 eV is most likely due to adsorbed CO. The high width of the C 1s peak centered at 284.5 indicates the contribution of several

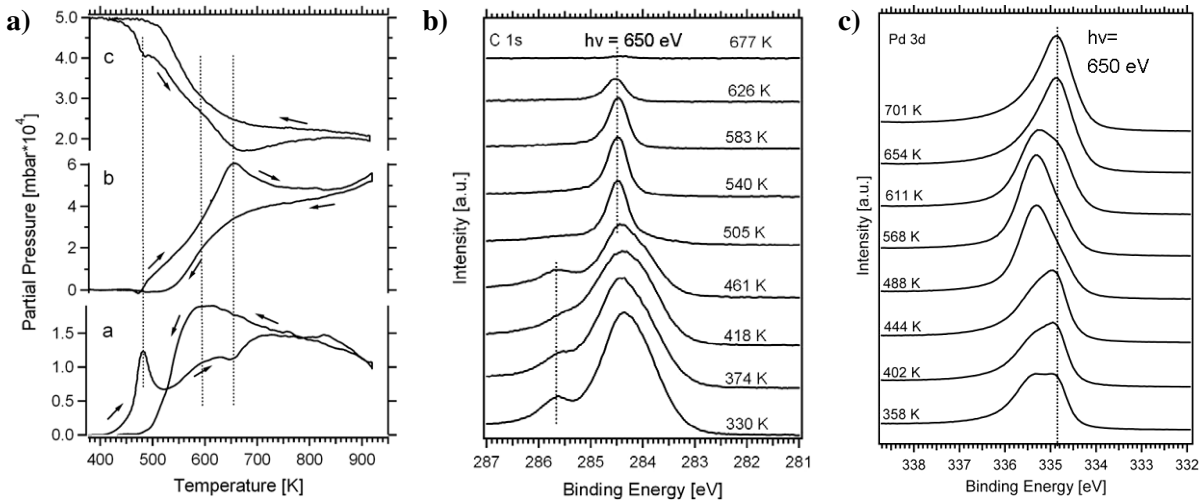

Figure 7. (a) Partial pressure of (a) CO_2, (b) CO and (c) ethene during the oxidation of ethene over Pd (111) plotted against temperature. (b) C 1s region recorded during heating from 330 to 670 K. (c) Pd $3d_{5/2}$ region recorded during heating. The photon energy for all XP spectra was 650 eV [30].

carbon species, a meaningful assignment of which is not possible here. However assignment of this peak to ethylidyne adlayers should be ruled out, since ethylidyne decomposes above 350 K [17, 32]. Between 461 and 505 K the C 1s spectrum changes completely. The broad peak between 283 and 285.5 eV and the CO peak at 285.65 eV disappear. Instead a sharp peak at the binding energy of 284.50 eV formed, indicating the presence of a single C species. The BE shift relative to adsorbed CO is in good agreement with calculations for dissolved carbon atoms [18]. This peak remains at a constant intensity up to 583 K, then vanishes above 677 K.

The Pd $3d_{5/2}$ spectra, shown in figure 7(c), are characterized by a peak at 334.9 eV assigned to the Pd bulk and a shoulder at higher binding energies in the temperature range from 358 to 444 K. The shape of the spectra changes strongly at higher temperatures. When the CO formation starts, the peak shifts to 335.4 eV and the peak becomes nearly symmetric. At 611 K the Pd bulk component contributes more strongly to the spectrum and above 654 K the spectrum becomes rather characteristic of clean Pd metal.

From the above described results it is evident that the ethene oxidation over Pd is catalyzed by two Pd phases, the metallic and an electronically altered phase, which is described by carbon dissolved in the Pd subsurface/surface region. The following explanation is proposed for the higher selectivity of the Pd–C phase to CO formation in the low temperature range. Since reactive carbon atoms are ubiquitously present in the dissolved carbon state of the catalyst, the steady state coverage of adsorbed oxygen may be rather low and a reduced lifetime of CO on the electronically altered surface may specifically favor the CO desorption pathway [17].

3.3. n-butane dehydrogenation on V based catalysts

Valorization of lower alkanes through dehydrogenation is an important process due to high demand for their unsaturated equivalents, which are widely used as a feedstock for commercial products. Dehydrogenation of light alkanes is achieved by the use of chromia or platinum based catalysts supported on alumina [33, 34]. However there has been a great deal of interest in the use of vanadia based catalysts for the (oxidative) dehydrogenation of light alkanes [35–40].

A major problem of dehydrogenation catalysts is loss of activity due to coking. This occurs readily due to the high temperature and low pressure required to achieve high yields of products. The thermodynamic limitations of the reaction can be overcome by addition of oxygen to the feed (i.e. oxidative dehydrogenation). The benefits of this are reduction in formation of coke and the ability to run the reaction at reduced temperatures. In the case of coke formation, the catalyst can be regenerated by treatment in oxygen at high temperature to remove the deposited carbon.

By the use of high pressure *in situ* XPS we have been able to probe the surface of a series of V_xO_y/alumina catalysts (1–8 wt% V/alumina) under dehydrogenation conditions (typically 0.4 mbar *n*-butane and 723 K). Reaction products were followed by mass spectrometry. In this case a proton transfer reaction mass spectrometer (PTRMS) and a quadrupole mass spectrometer were used to detect changes in the effluent gases while measuring spectra concurrently.

Figure 8 shows a typical reaction profile of *n*-butane dehydrogenation over 8 wt% V/alumina as measured by PTRMS. The major products detected were butene and butadiene (hydrogen evolution was followed by quadrupole MS). Figure 8(b) shows an enlargement of the low concentration products, which shows the formation of oxygenated products such as furan during heating to 723 K. As can be seen in figure 8, the maximum in formation of benzene corresponds to a change in slope of the butadiene formation. Hence, even at low pressures deactivation of the catalyst is observed. Since deactivation occurred at much slower rate at this low pressure, additional information can be gleaned from this 'slow-mo' view. Benzene has been detected as a minor product in a high pressure study of vanadium oxide/alumina

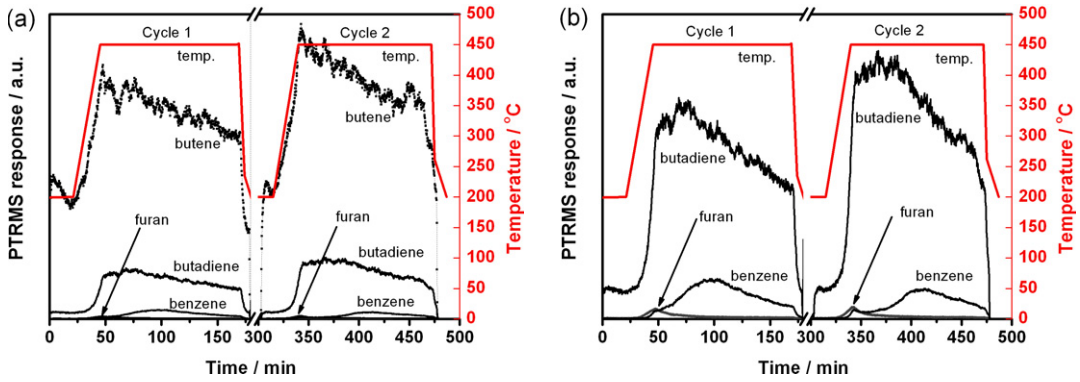

Figure 8. Reaction profile of 8% V/alumina catalyst under dehydrogenation conditions (0.4 mbar *n*-butane and 723 K) and an enlarged scale view of the low concentration products, denoted as (a) and (b) respectively. The products are assigned in the figures.

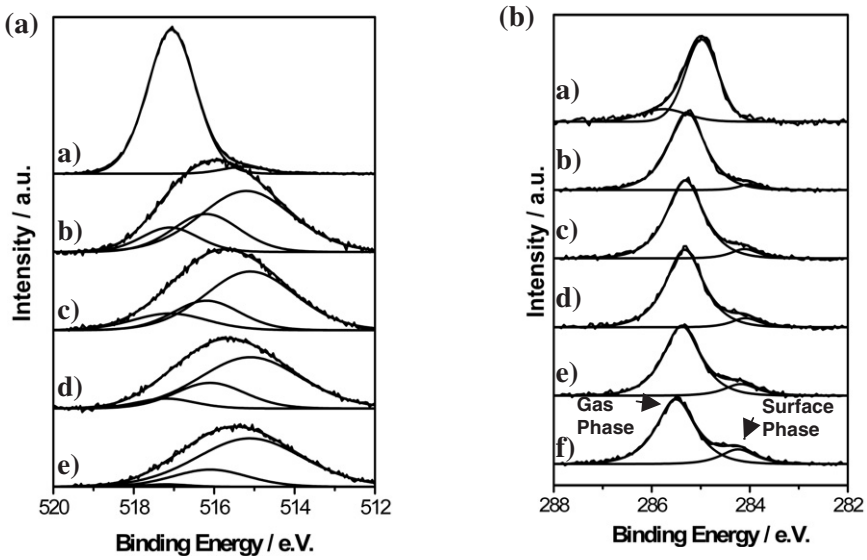

Figure 9. (a) XP spectra of the V $2p_{3/2}$ region during reaction of *n*-butane (0.4 mbar) over 8% V/alumina at 723 K, in (a) 0.5 mbar oxygen and 0.4 mbar *n*-butane after (b) 53 min, (c) 87 min, (d) 129 min and (e) 186 min. (b) XPS of the C 1s region during reaction in *n*-butane (0.4 mbar, 673 K) after (a) 60 min, (b) 96 min, (c) 114 min, (d) 118 min, (e) 134 min and (f) 174 min in the reaction mixture.

catalysts for butane dehydrogenation [36], and can form via the hydrogenolysis of the secondary–secondary C–C bond followed by oligomerization to benzene. Several authors have investigated zeolite based catalysts for the aromatization of *n*-butane to benzene [41–43]. Shpiro *et al* [42] described the formation of aromatic compounds from *n*-butane over Pt/Ga containing zeolites and Nguyen *et al* [43] combined kinetic and experimental results to determine the mechanistic steps. They suggest that the main route is through dehydrogenation to an alkene, followed by oligomerization, cyclization then dehydrogenation. These processes have also been described with regard to the coking mechanism of catalysts which is thought to proceed via the same steps [44].

At the same time, XP spectra of the V $2p_{3/2}$ core electron levels were measured under reaction conditions. Figure 9(a) shows the changes observed in the V $2p_{3/2}$ peak of the 8% V/alumina with varying reaction conditions. Under an oxygen atmosphere (0.5 mbar and 723 K), one relatively sharp peak was observed at 517.2 eV, the binding energy of which corresponds well with that of V^{5+} [45]. Only a small shoulder is observed on the low binding energy side of the peak, which suggests that less than 4% reduced vanadium is remaining in the oxidized catalyst. The catalyst was then treated in hydrogen (1 mbar, 723 K) and the contribution of reduced vanadium increased to around 30% of the V $2p_{3/2}$ peak (spectrum not shown).

Under dehydrogenation conditions, there is a distinct broadening of the V $2p_{3/2}$ peak and a shift to lower binding energy (figure 9(a)) due to reduction of V under reaction conditions. The broadening of the components assigned to the oxidation states which are commonly observed for V_2O_3 and V_2O_4 is due to the increased number of multiplet configurations available in the corresponding final states. The position of the peak in the final spectrum is 515.5 eV, which is in good agreement with the value given for V^{3+} [45]. It should be mentioned that fitting of the vanadium peak is non-trivial due to the broadening and varying binding energy calibration references that are used in the literature (e.g. valence band onset or internal standard). The spectra shown in figure 9 are fitted with three components corresponding to formal oxidation

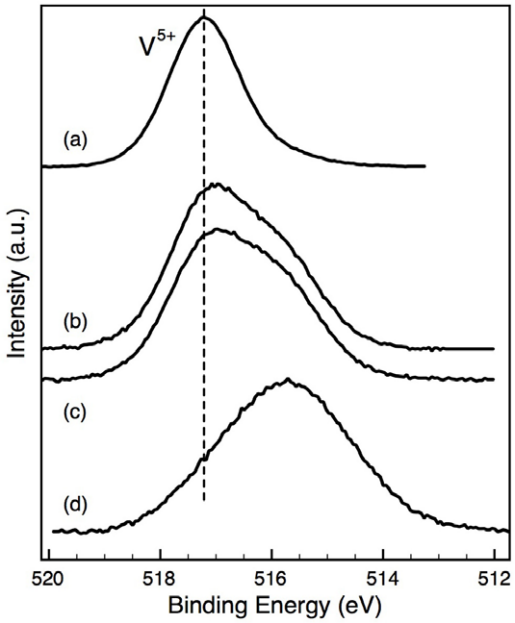

Figure 10. Comparison of V $2p_{3/2}$ XPS of 3.5% V/alumina in (a) 0.5 mbar oxygen, (b) 0.4 mbar 2% O_2 in *n*-butane, (c) 0.4 mbar 1% O_2 in *n*-butane and (d) 0.4 mbar *n*-butane.

states of 5, 4 and 3+ with binding energies of 517.1–2, 516.1–2 and 515.1–2 eV, respectively. The authors do consider this method to be consistent across a range of vanadium containing materials. In addition to the broadening and shifting of the peak, there is also a decrease in intensity of the V 2p feature compared to Al 2p signal of the support. This suggests that either the vanadium is preferentially covered by carbon or that there is agglomeration of the vanadium oxide particles during reaction which leads to a decreased contribution from vanadium.

Furthermore, distinct changes were observed in the C 1s region as shown in figure 9(b). Originally only the gas phase carbon peak is present. However during the dehydrogenation reaction this peak shifts, due to a change in work function of the sample as V reduced and carbon was deposited on the surface [46]. As the reaction starts to deactivate the intensity of the surface component increases. This increase correlates with a maximum in formation of benzene. Hence the carbon accumulation may be due to retention of benzene by the catalyst.

By relating the area of the peak corresponding to surface carbon with the average formal oxidation state as derived from peak fitting of the V $2p_{3/2}$ spectra; see figure 9 and the catalytic activity, a direct correlation can be observed between catalytic activity and vanadium surface electronic structure.

Figure 11 shows that the vanadium oxidation state decreases in parallel with increasing surface carbon. However the formation of butene and butadiene is not immediately effected by the formation of carbon on the surface. Only when the reduction of vanadium and formation of carbon reaches a certain extent does the dehydrogenation activity begin to decrease. Hence, it can be postulated that the deactivation occurs via two steps. Immediately on introduction of *n*-butane,

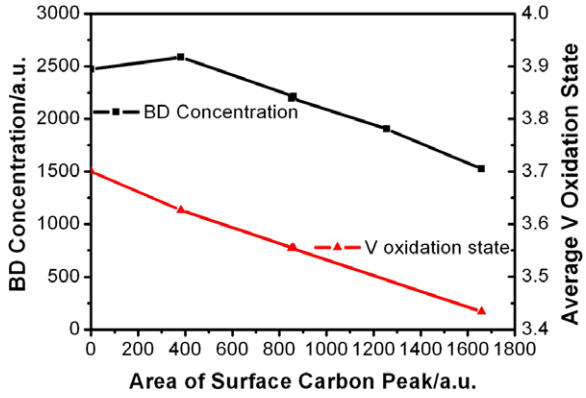

Figure 11. Structure–activity link between surface carbon, activity and oxidation state.

the oxidation state of vanadium is reduced; however it is not until after more than 60 min under reaction conditions that surface carbon is observed. Further retention of carbon (probably unsaturated hydrocarbons) requires multiple reduced vanadium sites, whereas their cumulative effect will result in catalyst deactivation.

As the catalyst deactivated carbon was formed on its surface during reaction, regeneration steps were used to determine the reversibility of carbon retention. After each regeneration (treatment in oxygen then hydrogen), the catalyst showed a higher activity towards the formation of butene and butadiene (as can be seen in figure 8). This was in agreement with the findings of Jackson *et al* [47] who investigated V_xO_y/alumina catalysts at high pressure (1 bar) for *n*-butane dehydrogenation and observed an increase in activity on subsequent cycles. During our investigation, three reaction cycles were performed over the catalyst. After regeneration, the surface was free of carbon. Vanadium XPS (not shown) at the same point during each dehydrogenation reaction showed that there was a slight increase in the oxidation state of vanadium after repeated regeneration and dehydrogenation cycles. Hence the maintenance of less reduced V (less V^{3+}) correlates with increasing dehydrogenation activity.

As part of our *in situ* studies, a 3.5% V/alumina catalyst was examined for the dehydrogenation of *n*-butane with and without 1–2% oxygen co-feed. Unfortunately addition of oxygen increased the formation of oxygenated products, including low concentrations of furan and dihydrofuran. However one possible benefit was the maintenance of V^{5+} as shown in figure 10 and that carbon was not observed on the catalyst surface. Hence, through control of the oxygen content of the feed gas it may be possible to balance the oxidation state of vanadium necessary for activity while reducing the formation of side-products.

From our *in situ* investigations, it is clear that reduced vanadium is active in the dehydrogenation of *n*-butane. However, as shown in figure 11 complete reduction to V^{3+} is not beneficial, as neighboring V^{3+} sites will bond adsorbates of C deposits too strongly. This is in agreement with the work of Harlin *et al* [36] who concluded that reduced vanadium was indeed active in the dehydrogenation reaction. By co-feeding

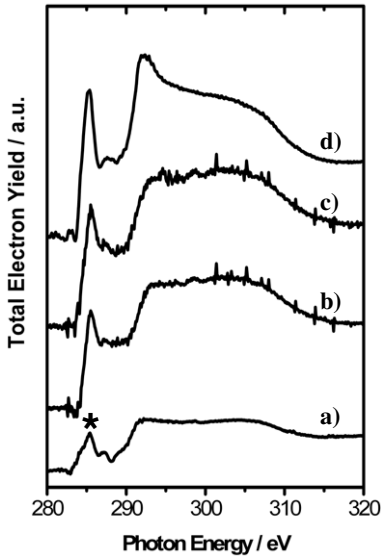

Figure 12. *Ex situ* post-reaction carbon K-edge NEXAFS of (a) 1% V/alumina, (b) 3.5% V/alumina and (c) 8% V/alumina *deactivated* during dehydrogenation of *n*-butane (1 bar) at 873 K and (d) graphite layer.

oxygen, a higher oxidation state of vanadium is maintained. Hence the presence of V^{5+} prevents accumulation of carbon on the surface. This effect of reducing carbonaceous deposits by co-feeding oxygen has been observed over Pt/alumina catalysts [48]. In the case reported, oxygen had two purposes: to fill high energy adsorption sites, allowing products to desorb, and to remove surface carbon, effectively cleaning the surface.

Measurement of the carbon K edge in the soft x-ray adsorption range provides useful information about the nature of deposited carbon which is difficult to ascertain from other spectroscopic methods. As mentioned earlier, less than 3% elemental carbon (determined by XPS) was formed on the surface of the catalyst during the low pressure reaction. Hence, post-reaction evaluation was also made of samples which were deactivated during reaction with 1 bar *n*-butane at 873 K as shown in figures 12(a)–(c). Vanadium XPS shows that the catalyst is greatly reduced (BE $\sim$ 515.9 eV). The main feature common to all of the carbon K-edge absorption spectra can be attributed to a 1s to π^* resonance due to the presence of unsaturated hydrocarbons. There were no distinct features in the 1s to σ^* region ($\sim$290–320 eV) which would indicate the formation of a well ordered form of carbon, such as in the case of highly ordered graphite [49]. The 3.5% V/alumina and 8% V/alumina had similar K edges, which corresponded to disordered carbon [50]. The 1% V/alumina catalyst showed however additional features on the low energy side of the main C 1s to π^* transition. Although not common, similar features were observed by Kolczewski and co-workers [51] and by Schlögl and co-workers [52] while investigating the absorption spectrum of styrene and ethylbenzene. Hence, the unexplained features of the absorption spectrum for the 1% V/alumina may be due to the presence of a styrene-like compound. This fits well with findings of a UV–Raman study into the deactivation processes during butane dehydrogenation over V_xO_y/alumina, which detected polystyrene-like intermediates during deposition of carbon on the surface [53]. Since the styrene-like features were only observed on 1%V, it is possible that the initial vanadium phase of mainly monomeric and dimeric species has an effect on the carbon species deposited. Additionally, variation of the intensity around 287 $\pm$ 1 eV is related to the presence of C–H bond orbitals [54]. Thus the nature of the carbon formed on the surface of the catalyst is affected by the catalyst loading and more likely the nature of vanadium oxide present i.e. isolated, polymeric and 3D V_2O_5 crystallites. This structure dependence on the nature of coke formation has been observed previously [44].

Hence, by combining *in situ* and *ex situ* spectroscopic experiments, it was possible to gain a greater insight into the dehydrogenation of *n*-butane and the subsequent carbon deposition. On addition of oxygen to the feed, surface carbon was not observed; however there was an increase in the formation of side-products. The additional maintenance of the V^{5+} species suggests that conserving a mixture of oxidation states is crucial to prevent deactivation, i.e. multiple neighboring reduced sites provide absorption sites for hydrocarbons, most likely unsaturated, causing coking and desorption hindrance for reaction intermediates [47].

Hess *et al* [56, 57] observed an additional feature in their XPS of V_xO_y/SBA-15 samples, at even higher binding energy than expected for V^{5+}. This was attributed to charging in the final state by the presence of small particles on an insulating support. Upon dehydration a dramatic change in the intensity ratio of the two V^{5+} components was observed as a result of a substantial increase in the vanadia dispersion.

In situ XPS proved to be a useful tool for identifying changes in vanadium oxidation state and deposition of carbon under reaction conditions. In the case of the vanadium/alumina catalysts, the presence of carbon appeared to have a negative effect on the formation of primary dehydrogenation products by blocking active sites required for catalysis.

The application of *in situ* XPS clearly demonstrated the dynamic character of the catalyst surface under changes of the reaction conditions. The formation a Pd–C phase in the selective hydrogenation of pentyne and the formation of partly reduced V sites during the dehydrogenation of *n*-butane were shown to be metastable. As soon as the gas feed was changed, the surface of the Pd and V catalysts changed.

4. Summary and outlook

The examples presented in this contribution show that the influence of C on the catalytic activity has a great variety. The formation of a carbon dissolved phase in Pd alters the electronic structure of the Pd surface. As shown in the 1-pentyne hydrogenation study, this phase disturbs the equilibrium between gas phase hydrogen and dissolved hydrogen, with strong influences on the selectivity. A very similar PdC phase was observed during the ethene oxidation over Pd. In this reaction the selectivity to CO is enhanced, when this special PdC phase is built up. In the case of the *n*-butane dehydrogenation the observed carbon deposit is correlated with deactivation of the V based catalyst. In this

case the carbon atoms seem to block the active sites of the dehydrogenation reaction. A co-feed of oxygen reduces the coking and thus prevents deactivation. However, it promotes the formation of side-products.

These case studies highlight the power of *in situ* XPS for the characterization of catalysts. The ultimate surface and element sensitivity on the one hand and the possibility of varying the information depth on the other hand adds an extra quality to XPS when operated at the synchrotron. In addition, x-ray absorption spectra (XAS) can be taken at a synchrotron to support XPS results. XAS is especially useful for gaining information about the geometric structure that is often hard to conclude from XPS results alone. This became obvious in the case of V based catalysts where C K-edge absorption spectra have been recorded to clarify the nature of carbon. The necessity for monitoring changes in the gas phase simultaneously with the spectroscopic characterization was demonstrated. By doing this, a correlation between surface and subsurface species with the catalytic performance of the catalyst was obtained. It became obvious that *in situ* XPS, though still limited to a certain pressure range (a few mbar), can be applied under relevant conditions to relevant materials.

Obviously, this raises the question of whether the pressure limit of *in situ* XPS might be enhanced further. In the following the physical boundaries of an XPS system based on a differentially pumped lens system will be discussed briefly.

Technically, pressures up to 100 mbar and higher might be handled with a differentially pumped electrostatic lens system. Certainly, the differential pumping needs to be organized in such a way that no electric discharge can occur inside the lens system due to an improper local gas pressure/voltage combination. A challenging problem is coping with the electron scattering within the vicinity of the first aperture of the lens system (on both sides of the aperture). Obviously, the path length of electrons in the gas phase needs to be minimized; i.e. the sample has to be located as close as possible to the first aperture of the pumping stages to reduce electron scattering. Due to the gas flow through the first aperture and the resulting local pressure drop in the vicinity of the aperture, the aperture diameter needs to be made small if the sample is moved close to it. This requires an adaptation of the x-ray spot size on the sample to the size of the aperture. The electron source, i.e. the illuminated area, i.e. the x-ray spot size, should not exceed the aperture size to have a high acceptance of the released photoelectrons. The creation of small x-ray spots in the μm range is feasible at modern third-generation synchrotron radiation sources like BESSY. The advent of fourth-generation sources, i.e. free electron lasers (FEL), will make even more intense small spot x-ray sources available. Nevertheless, small x-ray spots with high intensity (i.e. high photon density) might cause severe problems regarding the stability of adsorbed species or the integrity of the catalyst material itself (especially of oxide surfaces). Catalytically active surfaces need to show a high dynamic flexibility and response to the ambient conditions; thus these surfaces might be especially fragile. Although details of the mechanism of photon induced damage (e.g. changes of the physical structure and topography, molecular and electronic structure, and atomic composition) are still under discussion, beam damage is known to be a severe problem in studying non-conducting materials, polymers and organic materials [58, 59].

It seems obvious that every system under investigation needs to be carefully checked for these effects. There might exist individual pressure limits from this point of view for each system under investigation. Thus, a flexible experimental set-up that can be adapted to the needs concerning aperture diameter and x-ray density seems beneficial. Hard x-ray photoelectron spectroscopy might circumvent this issue partially and there is also a reduced scattering of high energy electrons with the gas phase (i.e. higher pressures are possible) but there is a lack of ultimate surface sensitivity due to the increased kinetic energy of the photoelectrons. Furthermore, avoiding a gas discharge inside the lens system might be somewhat problematic due to the higher voltages applied in the case of a high kinetic energy electron spectrometer.

Nevertheless, further development in detector technology and higher acceptance and enhanced transmission of future electrostatic lens systems certainly will increase the pressure limit of *in situ* XPS.

Furthermore, it was demonstrated in this report that the study of more kinetically demanding catalytic reactions is extremely useful. To tackle this topic, it seems necessary to incorporate the requirements for an adequate chemical reaction environment into the design of spectroscopic cells in order to mimic relevant conditions. Obviously, this is not an easy task, having in mind the classical layout of an UHV surface science electron spectroscopy experiment at a synchrotron source.

Beside the development of experimental techniques and equipment that allows for an advanced usage of modern electron spectroscopic techniques like *in situ* XPS, the access and handling of these stations needs to be improved to allow for a more general usage in the catalytic community. BESSY and the FHI recently installed a facility for tackling this problem. This facility named ISISS (innovative station for *in situ* spectroscopy) that started test operation at the beginning of 2007 is described briefly in the following.

ISISS consists of three main parts: (a) the *in situ* XPS end station that was used to obtain the results described in this report, (b) a state of the art soft x-ray beamline, and (c) the installation of a permanent infrastructure on site for experiments with a chemical background. The soft x-ray beamline is optimized to deliver photons in the energy range of 80–2000 eV, thereby allowing XPS of all relevant core levels. Additionally, it is possible to perform x-ray absorption measurements for a variety of important elements (e.g. K edges of light elements like carbon, nitrogen, oxygen, L edges of transition metals). Furthermore, the variation of photon energies over a reasonable extended energy range becomes feasible for performing depth profiling experiments as described in this report. Details of the optical layout of the beamline will be published elsewhere.

The availability of a permanent infrastructure on site for experiments with a chemical background is realized to be essential. In contrast to standard vacuum surface science experiments, *in situ* experiments require the installation of a

complex gas feed and elaborate gas analytics for determining the conversion of the gas phase during the reaction. Hazardous substances (e.g. poisonous or flammable) can be used much more safely with a permanent installation. Thus, the *in situ* XPS end station is completely covered in a ventilated housing big enough to operate it at ISISS. Thereby, all hazardous substances are separated from other synchrotron users in the experimental hall. This approach allows the effective installation of safety sensors if required. Another area in this housing gives the opportunity for easy and more complex sample pretreatments like calcinations, washing, drying, pelletizing etc. Obviously, a non-permanent infrastructure is either not capable of making such experiments possible or will be less safe, and much more time-consuming and costly in the long run.

It is expected that this facility will encourage the usage of *in situ* XPS for characterization of catalysts at BESSY in the future.

Acknowledgments

The authors gratefully acknowledge the BESSY staff for their continuous support during the experiments. Thomas Hansen is acknowledged for the TEM image of the alumina supported V catalyst. We thank the Deutsche Forschungsgemeinschaft (DFG) for the financial support through the Sonderforschungsbereich 546 and we also thank EPRSC of the UK and Johnson-Matthey plc for funding of the Athena Project.

References

[1] Siegbahn K, Nordling C, Johansson G, Hedman J, Heden P F, Hamrin K, Gelius U, Bergmark T, Werme L O, Manne R and Baer Y 1969 *ESCA Applied to Free Molecules* (Amsterdam: North-Holland)
[2] Joyner R W, Roberts M W and Yates K 1979 *Surf. Sci.* **87** 501
[3] Ruppender H J, Grunze M, Kong C W and Wilmers M 1990 *Surf. Interface Anal.* **15** 245
[4] Kelly M A, Shek M L, Pianetta P, Gür T M and Beasley M R 2001 *J. Vac. Sci. Technol.* A **19** 2127
[5] Pantförder J, Pöllmann S, Zhu J F, Borgmann D, Denecke R and Steinrück H-P 2005 *Rev. Sci. Instrum.* **76** 014102
[6] Ogletree D F, Bluhm H, Lebedev G, Fadley C S, Hussain Z and Salmeron M 2002 *Rev. Sci. Instrum.* **73** 3872
[7] Bluhm H, Hävecker M, Ihmann K, Kleimenov E, Teschner D, Ogletree D F, Salmeron M, Knop-Gericke A and Schlögl R 2008 *Rev. Sci. Instrum.* to be submitted
[8] Tanuma S, Powell C J and Penn D R 1994 *Surf. Interface Anal.* **21** 165
[9] Yeh J J and Lindau I 1985 *At. Data Nucl. Data Tables* **32** 1–155
[10] Himpsel F J, McFeely F R, Taleb-Ibrahimi A, Yarmoff J A and Hollinger G 1988 *Phys. Rev.* B **38** 6084–96
[11] Follath R and Senf F 1997 *Nucl. Instrum. Methods* A **390** 388–94
[12] Senf F and Sawhney K J S 2001 *Nucl. Instrum. Methods* A **467/468** 466–9
[13] Sawhney K J S, Senf F, Scheer M, Scheer F, Schäfers F, Bahrdt J, Gaupp A and Gudat W 2008 *Nucl. Instrum. Methods* A **390** 395–402
[14] Unterberger W, Gabasch H, Hayek K and Klötzer B 2005 *Catal. Lett.* **104** 1–8
[15] Han Y F, Kumar D, Sivadinarayana C, Clearfield A and Goodman D W 2004 *J. Catal.* **94** 131–4
[16] Bowker M and Morgan C 2005 *Catal. Lett.* **98** 67
[17] Gabasch H, Hayek K, Klötzer B, Knop-Gericke A and Schlögl R 2006 *J. Phys. Chem.* B **110** 4947–52
[18] Juddanov I V, Neyman K M and Rösch N 2004 *Phys. Chem. Chem. Phys.* **6** 116–23
[19] Rose M K, Borg A, Mitsui T, Ogletree D F and Salmeron M 2001 *J. Chem. Phys.* **115** 10927
[20] Teschner D, Vass E, Hävecker M, Zafeiratos S, Schnörch P, Sauer H, Knop-Gericke A, Schlögl R, Chamam M, Wootsch A, Canning A S, Gamman J J, Jackson S D, McGregor J and Gladden L F 2006 *J. Catal.* **242** 26
[21] Chastain J (ed) 1992 *Handbook of X-Ray Photoelectron Spectroscopy* (Minnesota: Perkin-Elmer)
[22] Teschner D, Pestryakov A, Kleimenov E, Hävecker M, Bluhm H, Sauer H, Knop-Gericke A and Schlögl R 2005 *J. Catal.* **230** 186
[23] Teschner D, Pestryakov A, Kleimenov E, Hävecker M, Bluhm H, Sauer H, Knop-Gericke A and Schlögl R 2005 *J. Catal.* **230** 195
[24] Daley S P, Utz A L, Trautmann T R and Ceyer S T 1994 *J. Am. Chem. Soc.* **116** 6001
[25] Ceyer S T 2001 *Acc. Chem. Res.* **34** 737
[26] Rupprechter G and Somorjai G A 1997 *Catal. Lett.* **48** 17
[27] Doyle A M, Shaikhutdinov S, Jackson S D and Freund H-J 2003 *Angew. Chem.* **42** 5240
[28] Khan N A, Shaikhutdinov S and Freund H-J 2006 *Catal. Lett.* **108** 159
[29] Haug K L, Burgi T, Trautman T R and Ceyer S T 1998 *J. Am. Chem. Soc.* **120** 885
[30] Gabasch H, Kleimenov E, Teschner D, Zafeiratos S, Hävecker M, Knop-Gericke A, Schlögl R, Zemlyanov D, Aszalos-Kiss B, Hayek K and Klötzer B 2006 *J. Catal.* **242** 340
[31] Surnev S, Sock M, Ramsey M G, Netzer F P, Wiklund M, Borg M and Andersen J M 2000 *Surf. Sci.* **470** 171
[32] Nishijima M, Yoshinobu J, Sekitiani T and Onchi M J 1989 *Chem. Phys.* **90** 5114
[33] Mimura N and Saito M 2000 *Catal. Today* **55** 173
[34] Shiau C-Y, Chen S, Tsai J C and Lin S I 2000 *Appl. Catal.* A **198** 95
[35] Blasco T and López Nieto J M 1997 *Appl. Catal.* A **157** 117–42
[36] Harlin M E, Niemi V M and Krause A O I 2000 *J. Catal.* **195** 67–78
[37] López Nieto J M 2006 *Top. Catal.* **41** 3–15
[38] López Nieto J M, Concepción P, Dejoz A, Knözinger H, Melo F and Vázquez M I 2000 *J. Catal.* **189** 147–57
[39] Mamedov E A and Cortés Corberán V 1995 *Appl. Catal.* A **127** 1–40
[40] Volpe M, Tonetto G and de Lasa H 2004 *Appl. Catal.* A **272** 69–78
[41] Kumar N and Lindfors L-E 1996 *Appl. Catal.* A **147** 175–87
[42] Shpiro E S, Shevchenko D P, Dmitriev R V, Tkachenko O P and Minachev K M 1994 *Appl. Catal.* A **107** 165–80
[43] Nguyen L H, Vazhnova T, Kolaczkowski S T and Luyanov D B 2006 *Chem. Eng. Sci.* **61** 5881–94
[44] Wu Z and Stair P C 2006 *J. Catal.* **237** 220–9
[45] Eberhardt M A, Proctor A, Houalla M and Hercules D M 1996 *J. Catal.* **160** 27
[46] Bluhm H, Hävecker M, Knop-Gericke A, Kleimenov E, Schlögl R, Teschner D, Bukhtiyarov V I, Ogletree D F and Salmeron M 2004 *J. Phys. Chem.* B **108** 14340–7
[47] Jackson S D and Rugmini S 2007 *J. Catal.* **251** 59–68
[48] McNamara J M, Jackson S D and Lennon D 2003 *Catal. Today* **81** 583–7

[49] Hitchcock A P and Mancini D C 1994 *J. Electron Spectrosc. Relat. Phenom.* **67** 1–132
[50] Fayette L, Marcus B and Mermoux M 1998 *Phys. Rev.* B **57** 14123–32
[51] Kolczewski C, Puttner R, Martins M, Schlachter A S, Snell G, Sant'Anna M M, Herman K and Kaindl G 2006 *J. Chem. Phys.* **124** 034302
[52] Joseph Y, Wuhn M, Niklewski A, Ranke W, Weiss W, Wöll C and Schlögl R 2000 *Phys. Chem. Chem. Phys.* **22** 5314–9
[53] Jackson S D, Rugmini S, Stair P C and Wu Z 2006 *Chem. Eng. J.* **120** 127–32
[54] Müller J-O, Su D S, Jentoft R E, Wild U and Schlögl R 2006 *Environ. Sci. Technol.* **40** 1231–6
[55] Su D S, Maksimova N, Delgado J J, Keller N, Mestl G, Ledoux M J and Schlögl R 2005 *Catal. Today* **102** 110–4
[56] Hess C and Schlögl R 2007 *Chem. Phys. Lett.* **432** 139–45
[57] Hess C, Tzolova-Müller G and Herbert R 2007 *J. Phys. Chem.* C **111** 9471–9
[58] Thomas J H 1998 *Beam Effects, Surface Topography and Depth Profiling in Surface Analysis* ed A W Czanderna, T E Madey and C J Powell (New York: Plenum) p 1
[59] Braga D and Grepioni F 2000 *Acc. Chem. Res.* **33** 601